CASL-U-2013-0326-000

Power uprates
and plant life extension

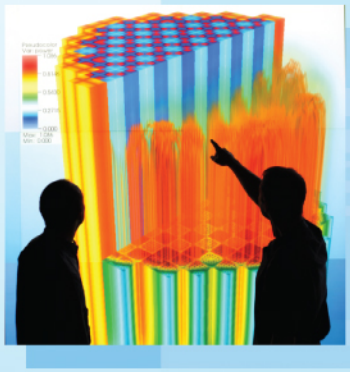

Engineering design
and analysis

Science-enabling
high performance
computing

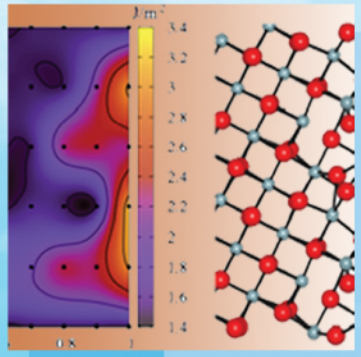

Fundamental science

Plant operational data

Consortium for Advanced Simulation of LWRs

L3:THM.ITM.P5.02
Bubbly Flow in Channel

Yassin A. Hassan and Carlos E. Estrada-Perez
Texas A&M University

October 31, 2012

U.S. DEPARTMENT OF ENERGY | Nuclear Energy

CASL-U-2013-0326-000

CASL REPORT: BUBBLY FLOW IN CHANNEL

Yassin A. Hassan
Carlos E. Estrada-Perez

Department of Nuclear Engineering
Texas A&M University
College Station, Texas 77843-3133
Phone: 979 845 7090
Email: y-hassan@tamu.edu

October 2012

CASL-U-2013-0326-000

ABSTRACT:

The purpose of this study is twofold: First, to perform measurements of turbulence and transport properties of a bubble-driven liquid flow within a square channel, and second, to provide best practice guidelines for the verification and validation of two-phase flow measurements.

To fulfill the first objective, time resolved Particle Tracking Velocimetry (PTV) and optical probe measurements were performed to investigate bubbles and liquid dynamics in a square channel. Among the measured parameters are included: whole-field liquid and bubbles velocities, velocity fluctuations, and Reynolds stresses. Also are provided dispersed phase parameters such as local void fraction, bubble size distribution, bubble frequency and bubbles average and instantaneous velocities.

The second objective was fulfilled by performing a sensitivity analysis of the parameters influencing the accuracy of the measurements. Errors quantification and best practice guidelines were obtained from this analysis to provide meaningful flow descriptive statistics with higher accuracy and reduced errors. This study was an effort to provide data for verification, validation, and improvement of two-phase flow numerical simulations.

Experiment description

The experimental rig consisted of a liquid container tank, a laser illumination system, a high speed camera, a halogen lamp and a square channel test section (See Fig. 1(a)). Details of the relevant components are given in the next paragraphs. The liquid container was made out of glass with a wall thickness of 1.27cm, and served as a phase separator and as an optical correction box. The tank inner dimensions are 91.44 cm in length, 30.48 cm in width, and 63.50 cm in height. Two holes with a diameter of 2.54 cm were made at the tanks' bottom to allow piping access for air injection and drainage. The water was supplied from a nearby line at room temperature (20-22 °C). The tank was filled with 48.26 cm of water and all measurements were taken with stagnant water conditions. Air was injected through a porous media disk at the tanks' bottom. The pores on the disk ranged from 40-60μm.

Air was injected at a constant temperature of about 22 °CC (Room Temperature), and a constant pressure of 35 psig. A high efficiency particulate air (HEPA) filter was placed in the path of the air-flow to prevent any debris from entering the test section. Three superficial gas velocities (j_g) were applied to produce the bubbly flow: 4.6 mm/s, 2.5 mm/s, and 1.4 mm/s. The superficial gas velocity was defined as

$$j_g = \frac{Q_g}{A} \tag{1}$$

where Q_g is the gas volumetric flow rate and A is the flow area before entering the porous media. The flow rates were chosen to study a range of different bubble sizes and velocities. A flow meter, ranging from 0-100 mL/min, placed in the flow path allowed viewing and setting the flow rates.

The test section was a square channel with a hydraulic diameter (D_h) of 2.2 cm made out of transparent acrylic with a wall thickness of 0.16 cm, and 61 cm length. Two small slots were milled on one of the sides of the channel allowing the optical probe to enter the channel. Excess room was covered around the slots when the probe was positioned for measurements.

The high speed camera used for the visualization experiments provided a resolution of 1024 pixels x 1024 pixels with a time interval between two consecutives frames (ΔT_{PIV}) of 1ms. The flow within the test section was seeded with fluorescent particles of 30 μm. The laser light used to excite the particles' fluorescent emission was an Nd:YAG with a 532 nm laser light wavelength. With this excitation (532 nm), the particles fluorescent light wavelength peak was aroung 580 nm. The difference in wavelengths between the fluorescent emission and laser excitation light provided a means of filtering the laser light reflections from walls and bubbles. This was achieved with a narrow band optical notch filter designed to reflect the laser light wavelengths and to transmit the fluorescent emitted light from the tracer particles.

The camera was installed on translational stages that were controlled via a computer, making it convenient to switch between measuring regions. For each region of interest, measurements were performed with PTV, shadowgraphy, and the optical probe sensor.

The experiment focused on two different regions far from the inlet where high-magnification studies were performed (see Fig. 1(b) for region positions). The regions coincided with the location of the slots milled for the probe entrance. For each region, two types of experiments were performed: First, PIV experiments focused to measure the effect of void fraction on the liquid dynamics and second, shadowgraphy and optical probe sensor experiments which focused on measurements of the gas phase dynamics.

It should be noted that in order to avoid intrusiveness between shadowgraphy and the optical probe sensor measurements, the shadowgraphy measurement area was slightly below the optical probe sensor position. This ensured that the bubble-probe interactions would occur above the shadowgraphy region and cause no erroneous measurements in shadowgraphy analysis. The area covered by the camera for both regions was 2.2 cm in width and 1.5 cm in height. The probe was kept at heights of 36.8 cm and 40.6 cm when measuring regions 1 and 2, respectively. (see Fig. 1(b))

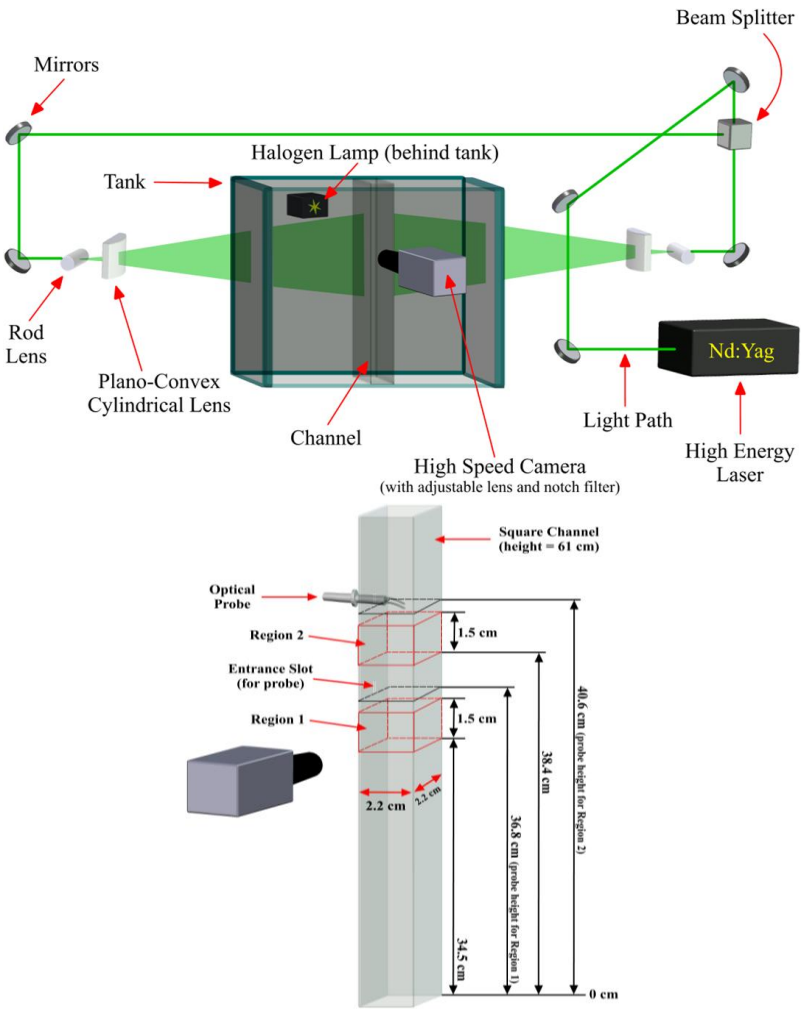

(a)

(b)

Figure 1: Schematic of experimental facility and test section.

RESULTS

Although two regions were studied in this experiment, in this report we will present the results of the region with more flow developing distance (see Figure 1(a)). Figure 2 and 3 show the Reynolds shear stresses for the gas and liquid phases in both regions for the largest flow rate (j_g = 4.6 mm/s). The small discrepancy between both regions is an indication that fully developed flow was achieved for both phases at the measurement regions position.

Visualization experiments parameters optimization

Optimizing time interval between image pairs

Sensitivity experiments were performed to obtain optimal timing parameters for the visualization experiments. The required parameters included the time interval between two consecutive image pairs (ΔT_{PIV}), and the straddling time (ΔT_{str}). These parameters showed to have a high impact on the quality of the measured flow statistics.

The procedure was as follows: First, the images were recorded continuously at 1000 fps resulting in 10,918 images (maximum internal camera memory). Figure 4 shows the bubble centroid velocity as a function of the distance from the center of the channel (x = 0 mm). The velocity profile obtained under these conditions did not show the smooth tendency expected on this types of flows. In order to reduce the irregularities found in the velocity profile, a higher bubbles sampling was required. Usually, an increase in the sample number improves the statistics of the study. A bubble entering the region was tracked approximately 115 times before exiting. Thus,

an effort was made to change the sample number of the bubbles – the bubbles that appeared in the image pairs. Tracking each bubble once instead of multiple times was desired.

Next, the images were captured in sets. The camera memory was partitioned into 64 sets each able to record 170 continuous images at 1000 fps. The camera was triggered every 15 seconds with a signal to record each set. This method ensured that a new sample of bubbles was observed after each set. As Fig. 4 shows, the results did improve, but large fluctuations were still present in the profile. Finally, it was decided to have a new sample of bubbles after each pair of images (it is required to have at least two consecutive images for tracking purposes). The camera was triggered to capture only two images every 0.2 seconds because it took approximately 0.115 seconds (115 images at 1000 fps) to allow a completely new set of bubbles to enter the visualization region. Again, a total of 10,918 images were captured (5,459 image pairs). Figure 4 shows how this method significantly improved the velocity profile. Notice how the continuous data profile is below the other profiles. This change indicates that using consecutive images may lead to incorrect velocity estimation due to the small amount of samples used to obtain the velocity. Even though the profiles had improved, one set of 5,459 pairs was not sufficient. Five sets were captured in order to reduce the uncertainty in the measurements, 54,590 images (27,295 image pairs).

The sensitivity study vastly assisted in improving the velocity profiles, among other statistics not mentioned here. This study proved that it is recommended to have a different sample or inventory of bubbles present after each image pair. After performing this study, all the following measurements employing PTV and shadowgraphy had a sufficient time interval between image pairs to guarantee observation of a new set of bubbles.

Discrepancy between probe and shadowgraphy

Another important aspect was the discrepancy between the parameters provided by the optical probe and shadowgraphy. The optical probe measured higher velocity values and lower void fraction values than shadowgraphy. The two methods provide similar parameters through different techniques.

The optical probe calculates the bubble velocity based on the detection of the bubble surface, since it is the point of contact for the probe tip. The interface velocity is calculated by dividing the distance between the probe tips by the time it takes for the bubble surface to travel from one tip to the next, whereas shadowgraphy calculates the velocity by tracking the centroid of the bubble. Furthermore, the probe is a point measurement technique while shadowgraphy is a 2-D method. The probe velocity calculation presents a problem because the bubble surface is constantly deforming and deforms even further when the bubble interacts with the probe. Also, the probe may not contact the bubble directly in the center. On average the bubble centroid has a smaller displacement than does the bubble surface. Since the surface is moving faster than the centroid, the velocity resulting from the probe is larger compared to the one obtained with shadowgraphy. In Fig. 5, two cases of bubble-probe interaction are shown. The bubble centroid and interface are shown separately in consecutive images A and B, while image C shows the two images (A and B) superimposed. Image C from both cases reveals the average axial displacement and a larger difference is seen for the bubble surface. Note that the squares in the images represent an approximate location of the bubble centroid and surface.

Shadowgraphy presents an issue calculating the velocity and void fraction due to a dimensional disagreement. The problem encountered in shadowgraphy is the representation of a 3-D region as a plane (2-D). The method captures all the bubbles in the region of interest (which is a volume) but shows a planar view of that region. Even though the velocity in the central plane of the channel is desired, the calculated velocity is an average of multiple planes throughout the channel where the bubbles exist. Due to this issue, the void fraction will be much larger when calculated by shadowgraphy as all the bubbles in the 3-D volume are captured into a 2-D image. For example, if there were only five bubbles in the plane of interest shadowgraphy images may show greater than ten bubbles. It is believed that the aforementioned phenomena cause the discrepancy between the two methods.

Optical probe and shadowgraphy results

The optical probe and shadowgraphy provided gas phase parameters. Figure 6 shows the average void fraction distribution across the channel for the different flow rates. There is an increase in the void fraction closer to the wall than the center. This peaking is due to the lift force that occurs close to the wall (Mudde et al., 2008). Low values of the void fraction were observed due to the point measurements along a line from the optical probe. The void fraction profiles provided by shadowgraphy are shown in Fig. 7. The distributions have higher magnitude than the ones obtained from the optical probe. The discrepancy regarding the dimensional disagreement causes the large difference in the void fraction. The profiles exhibit a similar shape found in the optical probe results confirming that the majority of the bubbles are distributed closer to the wall. It can be seen from the figures that as the flow rate is decreased the void fraction also decreases, since the size and amount of bubbles become smaller in the channel.

The bubble interface velocity obtained from the optical probe is shown in Fig. 8. Observe the decrease in the value as the distribution approaches the wall. The bubbles take a longer time to travel from one probe tip to the other when they are closer to the wall leading to a decrease in the velocity near the wall (v=d/t; d is constant at 1.4 mm). A decrease in motion will occur from the bubble-wall interaction. It was visually confirmed that the bubble motion was significantly reduced when they collided with the wall. According to the void fraction plots, bubble to bubble interactions will also occur because of the void fraction peaking near the wall and may be another reason why the interfacial velocity decreases. Figure10 shows the average bubble centroid velocity distribution for the three flow rates. Note that the velocity profiles are increasing as the flow rate decreases (similar to bubble interface velocity from probe). The same explanation given for the optical probe can be applied here. There is a dip in the center of the distribution in Fig. 9 for j_g = 1.4 mm/s. It can be attributed to the low amount of bubbles that were present in the center of the channel. In the small flow rate case many small bubbles ranging from approximately 360 – 480 μm emerged from the porous media and remained mainly in the center. Even if there are larger bubbles traveling faster in the center of the channel, the tiny bubbles form a cluster with the larger bubbles and the cluster is tracked as one bubble. The tiny bubbles also formed clusters. The extremely slow velocity of the tiny bubbles reduced the average centroid velocity and leads to a dip near the center. Comparing the heights of the profiles from Figs. 8 and 9, we see that the bubble interfacial velocity is greater than the bubble centroid velocity. This is due to the discrepancy mentioned earlier.

The velocity profiles shown in Figs. 8 and 9 increase with decreasing flow rate. The opposite may be expected as larger bubbles are thought to travel faster due to their size. However, the results show that larger bubbles have the lowest average velocity. This may be

caused by surface deformations of the larger bubbles. Another explanation may come from the forces acting on the bubble. Larger bubbles have less surface tension (per volume) and are more buoyant compared to smaller bubbles. They oscillate more frequently than smaller bubbles and the surface is constantly deforming. Small bubbles do not have surface deformations on the same scale as do large bubbles. Although they are less buoyant, less frequent oscillations may allow them to travel faster. Both types of oscillations for the two bubble sizes were visually confirmed.

The trend of increasing velocity with decreasing flow rate may be due to a certain size range present from the flow rates chosen for this experiment. From this study the results showed a greater velocity for smaller bubbles than for larger bubbles. This does not infer that if the flow rate is reduced further, bubbles smaller than the current size will travel faster. Similarly it does not infer that bubbles larger than their current size will travel slower if the flow rate is increased further.

The Sauter mean diameter (Fig. 10) was not found to have any particular pattern as the flow rate decreased other than the decrease in the average size and increase in the average uncertainty. It was expected that the bubbles will become smaller as the flow rate was reduced, which is shown in the figures. The increase in the uncertainty implies larger variation in the bubble size as the flow rate decreases. Bubble size was also estimated from shadowgraphy (Fig. 11). The size was based on the assumption that the bubbles were spherical (circular in 2-D view). The figure shows the size to decrease as the flow rate decreases. The same trend was found in the Sauter mean diameter measured by the optical probe, confirming that the bubbles become smaller as the flow rate is reduced. For each flow rate, the size is fairly constant after which the profiles drop quickly. This indicates that the larger bubbles in a given flow rate tend to remain in the central region of the channel, whereas the smaller bubbles remain close to the wall.

Turbulence related results from visual methods

The tracking algorithm applied to the visual methods (shadowgraphy and PTV) was able to provide turbulence related parameters such as the fluctuating velocity for each component (u', v') and the Reynolds shear stresses. The full channel region was considered for both parameters. The fluctuating velocity signifies the degree of variation in the instantaneous velocity from the average velocity. In other words, large values would occur from large fluctuations in the flow due to the constant change in the instantaneous velocity. Studying and measuring turbulence parameters is vital in understanding two-phase flow behavior. Experimental parameters are necessary for turbulence modeling and, in general, for improving and validating simulations.

Although there was no liquid flow in the channel, the liquid movement was caused by the bubbles. As can be seen in Fig. 12, the liquid motion is negligible compared to the bubble motion. Since all average liquid velocities are less than 2.0 % of the average bubble velocities, the remaining liquid velocities are not shown.

The fluctuating velocity of the bubbles is given in Fig. 13. The high and medium flow rates seem to have a fairly constant profile in the center of the channel whereas the low flow rate shows a change in the profile, especially for v'. Also note how the values of u and v change as the flow rate is decreased: u decreases and v increases. This means that the fluctuations of the radial component of the velocity decreases and those of the axial component increase. It suggests that larger bubbles oscillate more frequently than smaller bubbles in this case.

The fluctuations in the axial and the radial components of liquid velocity were provided by the root mean square, shown in Fig. 14. Notice the decrease in the values of the fluctuations as the flow rate decreases. Due to the large liquid disturbance caused by the large bubbles, the fluctuation value is highest for j_g = 4.6 mm/s. On the other hand, smaller bubbles will cause

smaller liquid disturbance. Therefore the low flow rate has the lowest fluctuation values. The axial component of the fluctuating velocity has larger values than the radial component for all three flow rates meaning that the variation in the liquid velocity is larger in the axial direction than the radial direction. Since the bubble motion is mainly in the axial direction, the effect on the velocity fluctuations will be in the same direction.

The Reynolds shear stresses obtained from shadowgraphy are shown in Fig. 15. The figure shows large changes near the walls. This may be due to the large velocity gradient occurring in that area (see the large difference in the centroid velocity from x=7-11 mm in Fig. 9). Note the increase in the peak values as the flow rate decreases. The Reynolds stresses show that as the flow rate decreases the bubble centroid velocity increases and causes a larger velocity gradient close to the wall. An interesting observation from Fig. 15 is the comparatively flat profile in the center of the channel for j_g = 1.4 mm/s. Even though the velocity distribution in Fig. 9 shows a slight increase in the center of the channel, there seems to be no indication of that in the Reynolds shear stress. It may be due to the low magnitude of the gradient near the center compared to the high gradient near the wall.

The Reynolds shear stresses obtained from PTV are shown in Fig. 16. They show a changing profile throughout the channel. The largest values occur from the highest flow rate due to the largest liquid displacement. As the flow rate is reduced, the profile decreases indicating that there are fewer fluctuations in the liquid velocity.

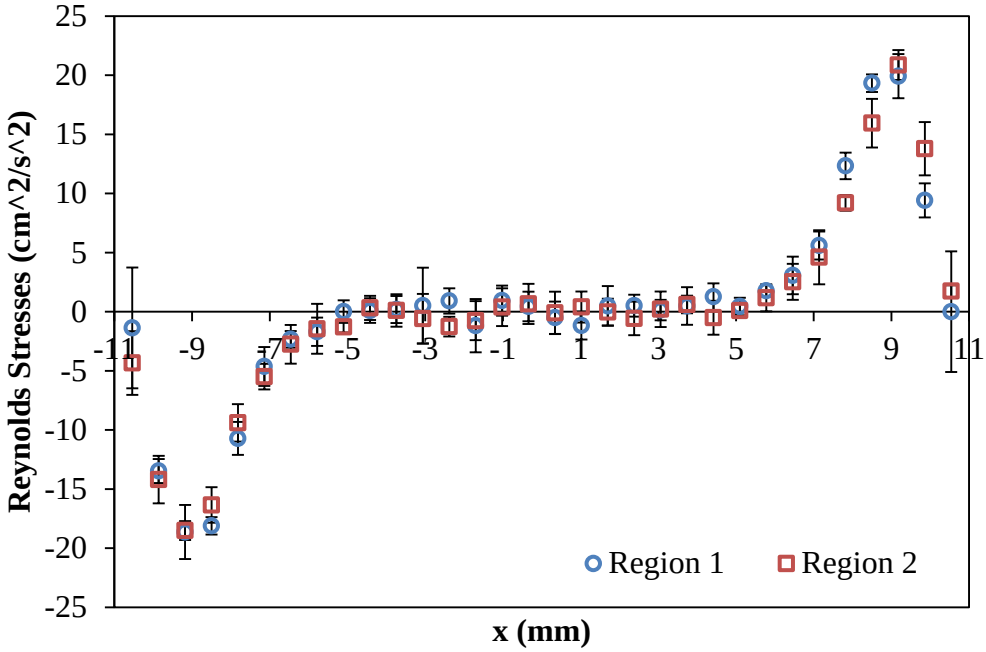

Fig. 2: Bubble Reynolds shear stresses obtained from both regions.

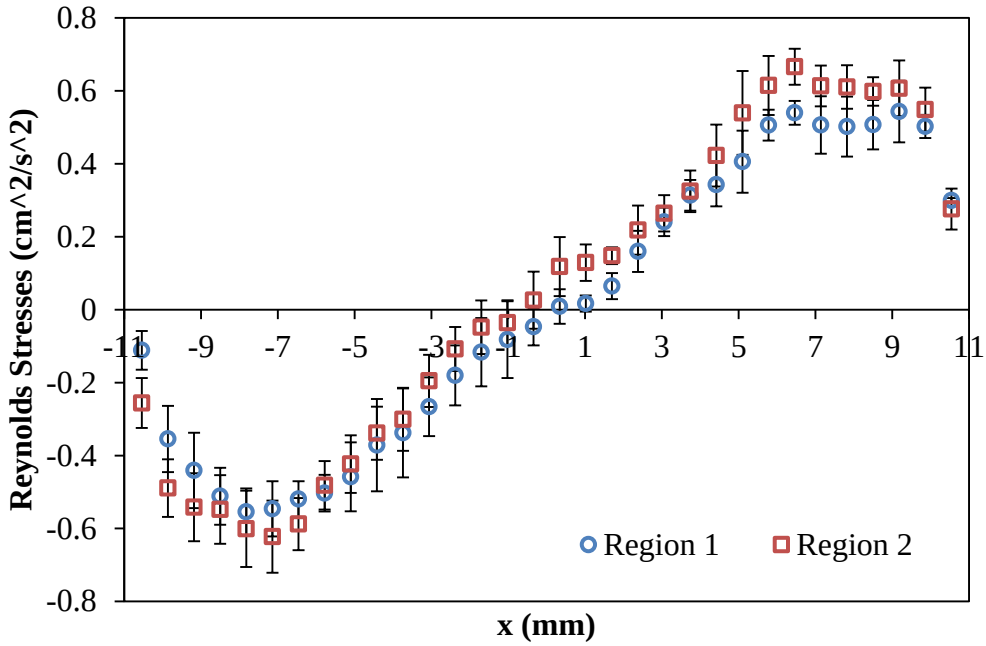

Fig. 3: Liquid Reynolds shear stresses obtained from both regions.

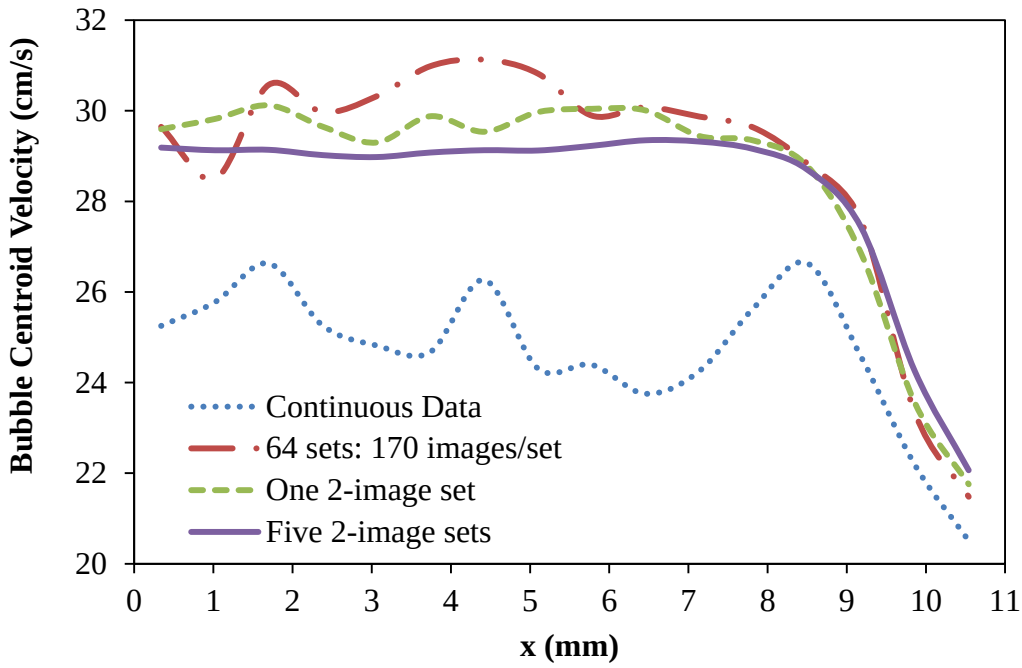

Fig 4: Sensitivity study showing different bubble centroid velocity profiles by varying duration in between image sets.

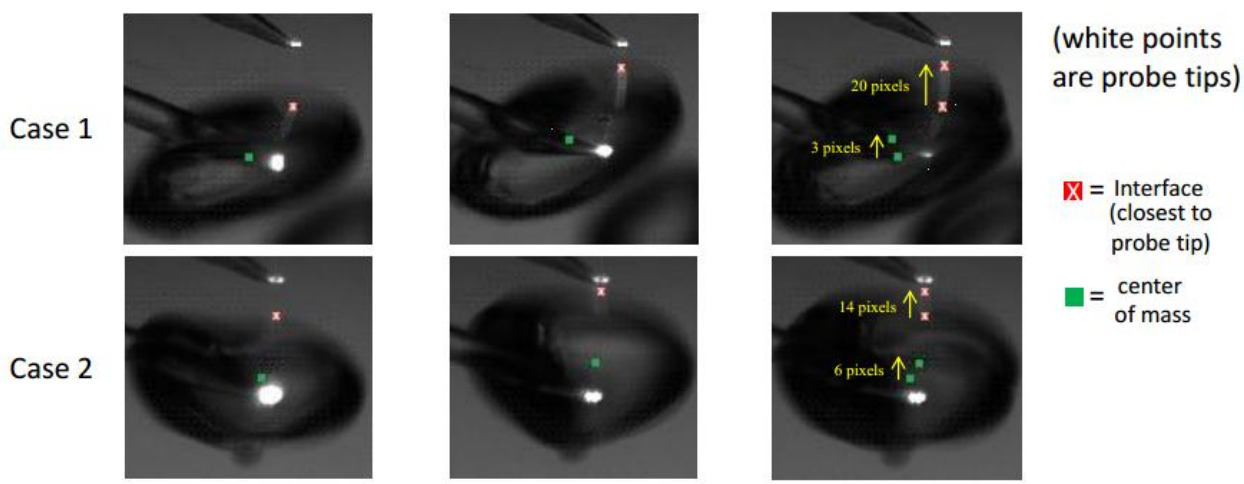

Fig 5: Estimation of discrepancy between bubbles velocity measurements using the optical probe sensor (interface velocity) and shadowgraphy (center of mass velocity).

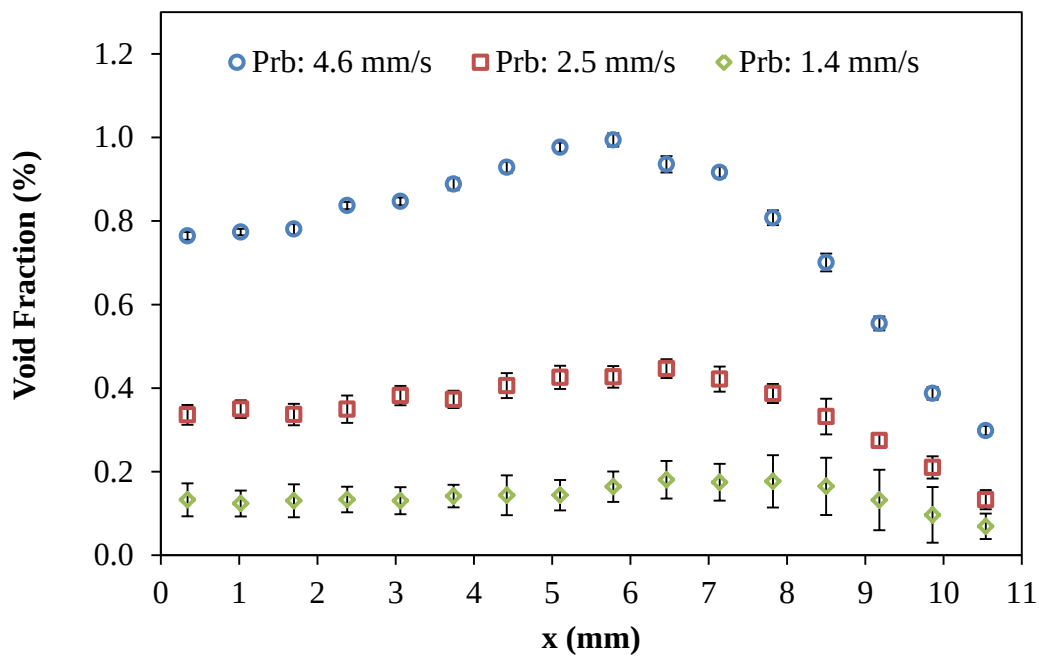

Fig. 6: Void fraction obtained from optical probe.

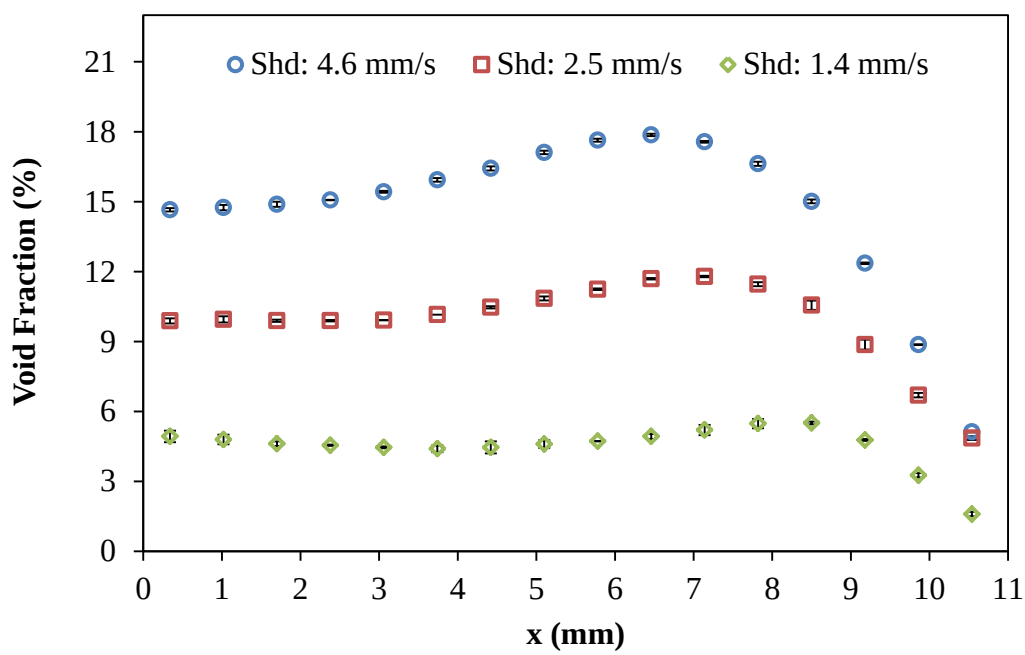

Fig. 7: Void fraction obtained from shadowgraphy.

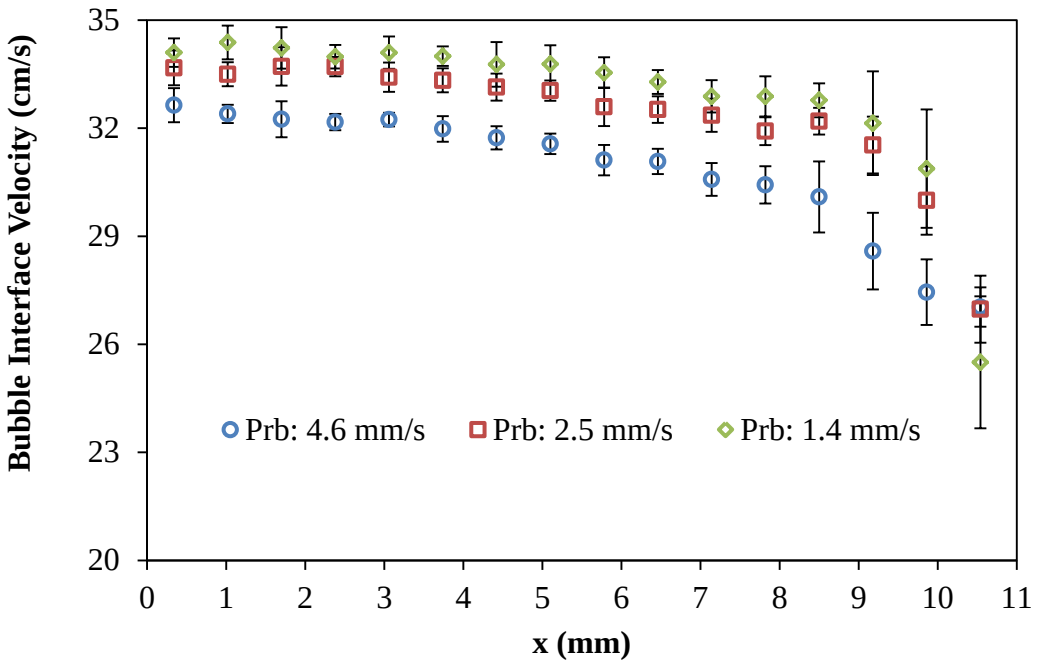

Fig. 8: Bubble interfacial velocity obtained from the optical probe.

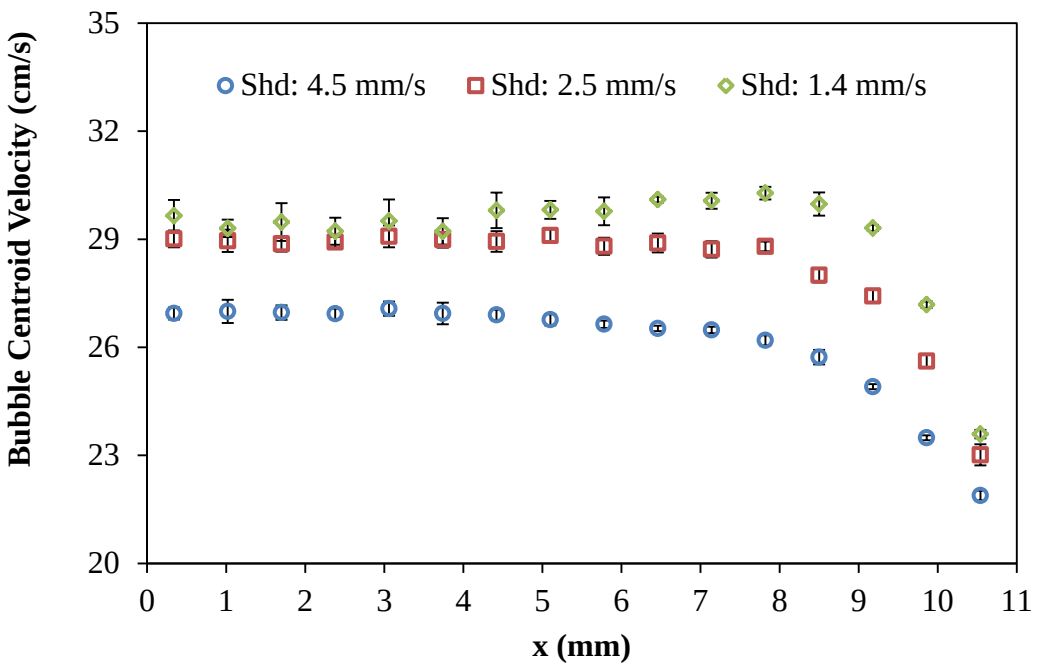

Fig. 9: Bubble centroid velocity obtained from shadowgraphy.

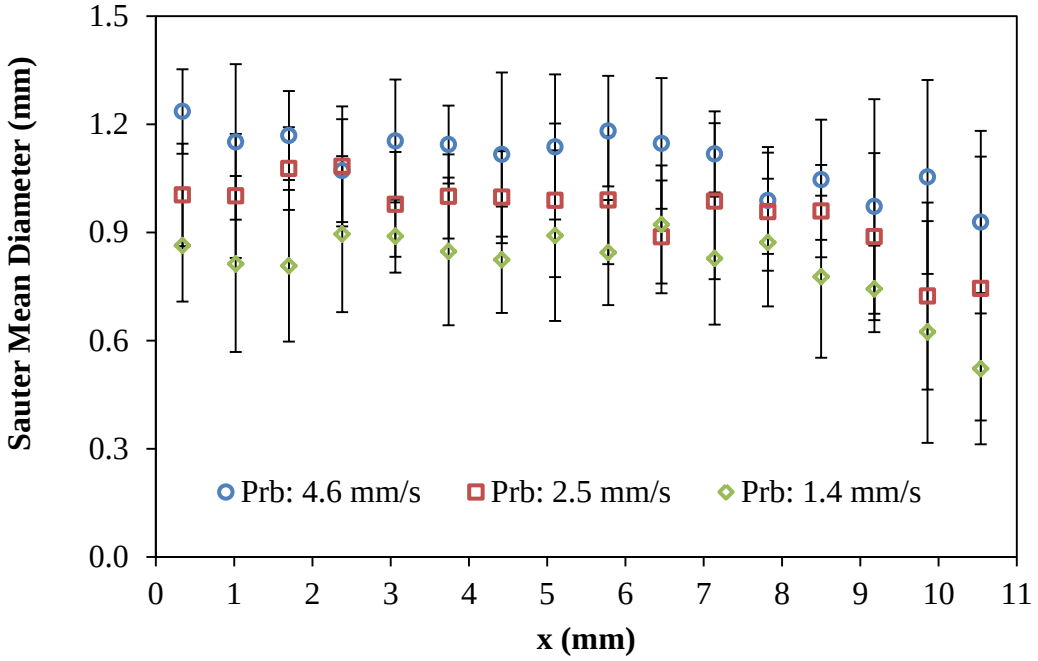

Fig. 10: Sauter mead diameter obtained from the optical probe.

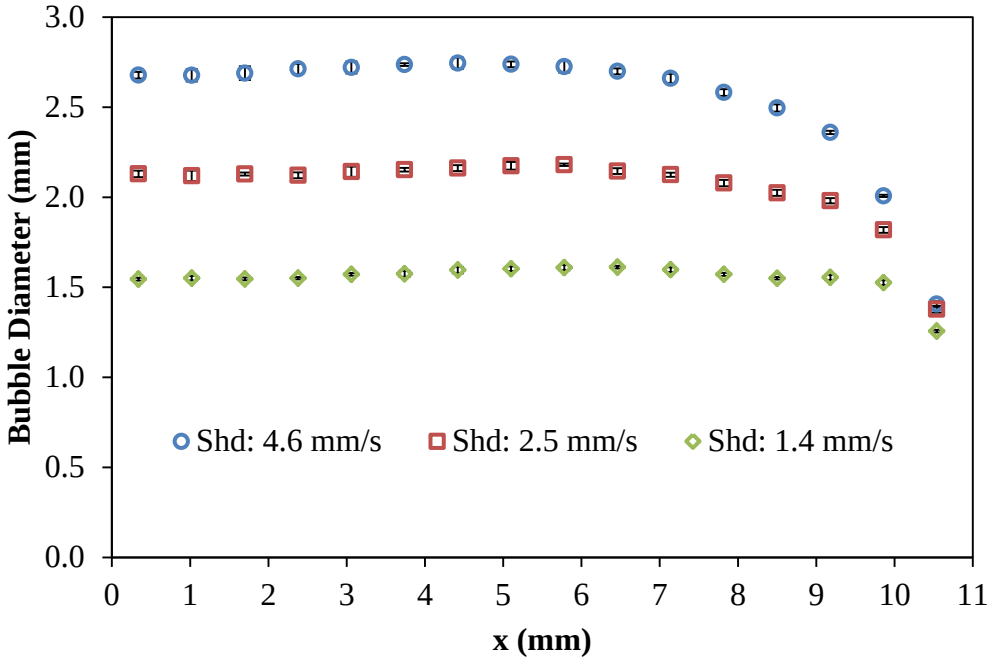

Fig. 11: Bubble diameter obtained from shadowgraphy.

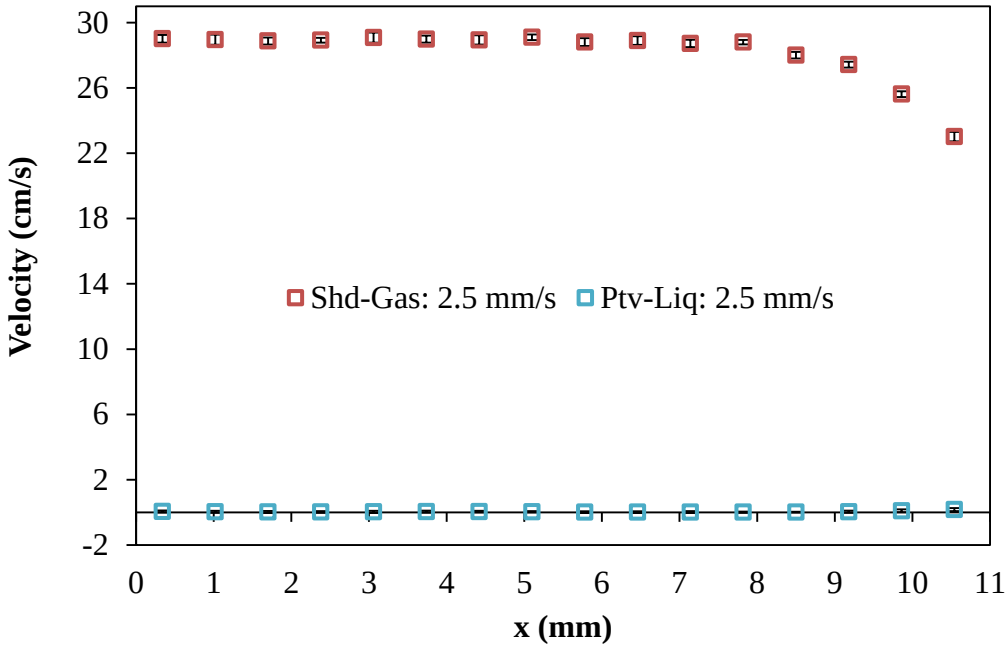

Fig. 12: Liquid velocity shown to be negligible compared to gas velocity.

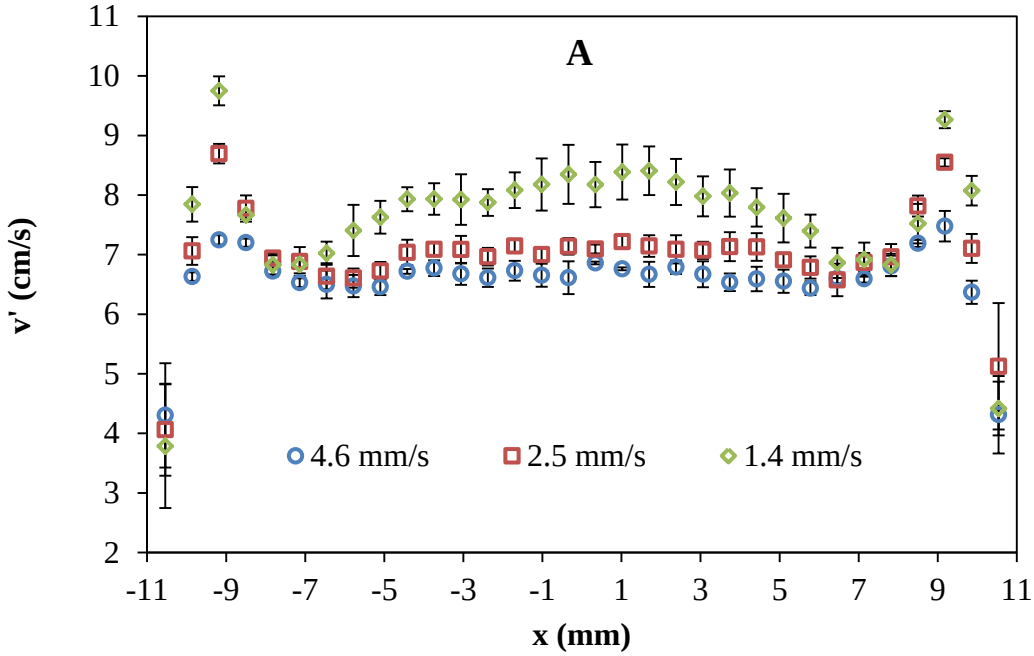

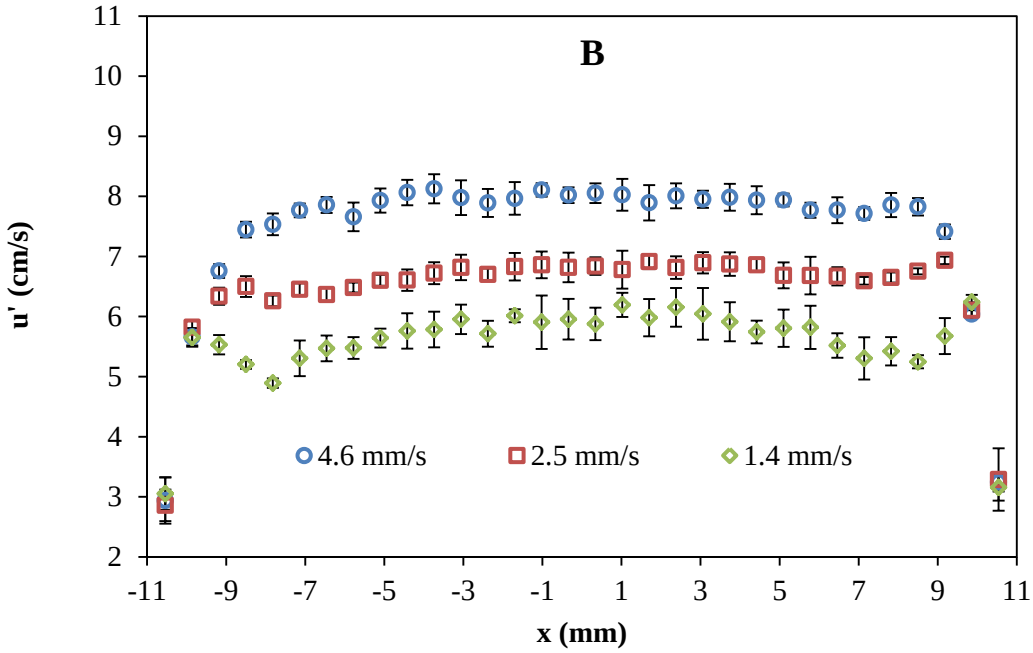

Fig. 13: Fluctuations in the bubble velocity: A) axial, B) normal.

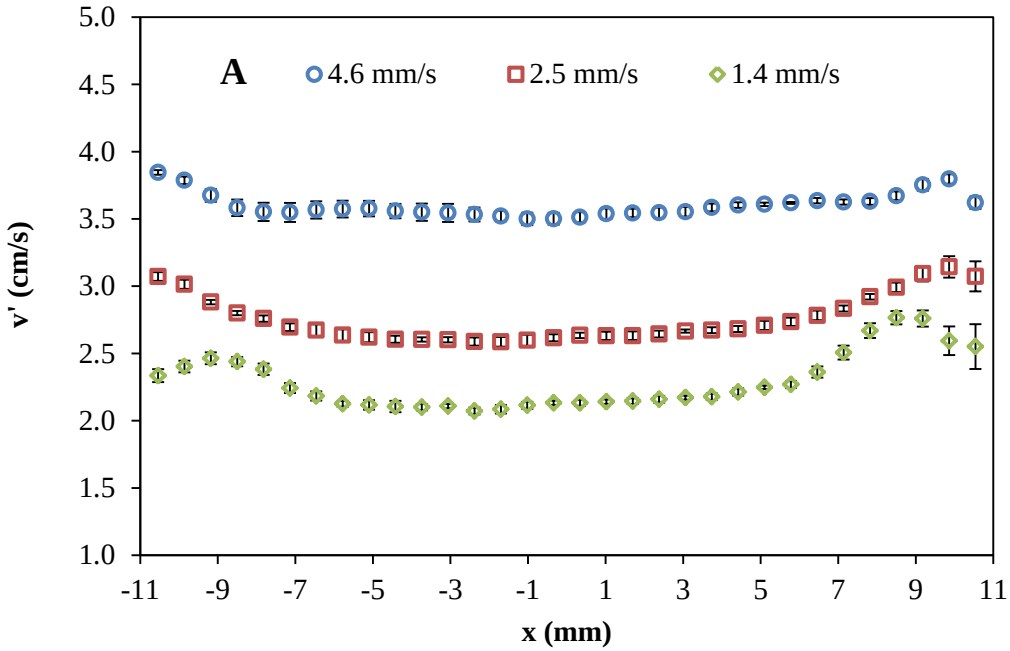

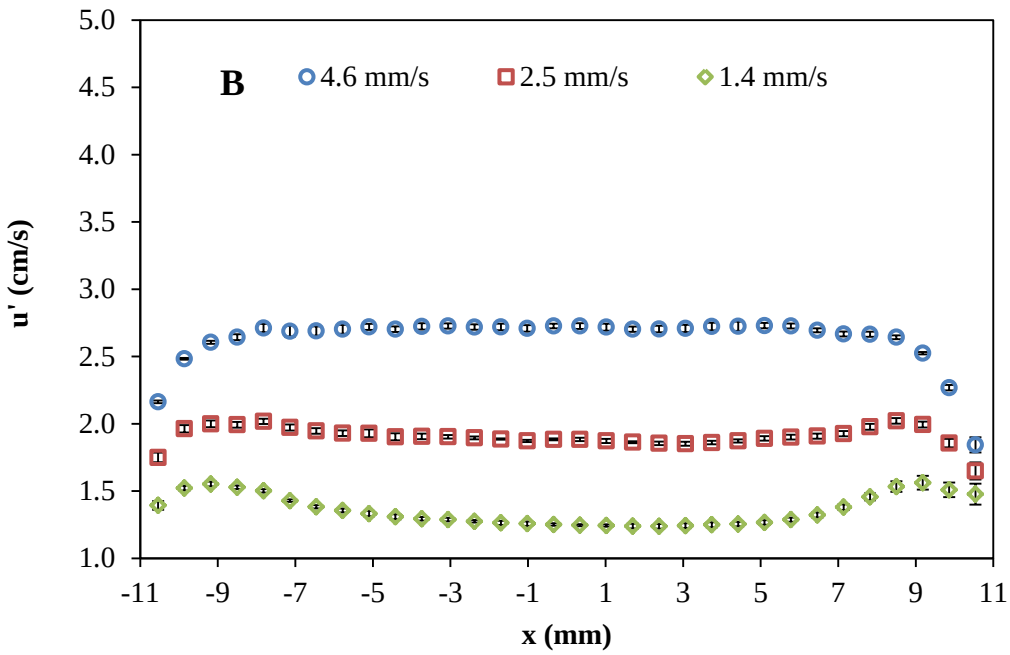

Fig. 14: Fluctuations in the liquid velocity: A) axial, B) radial.

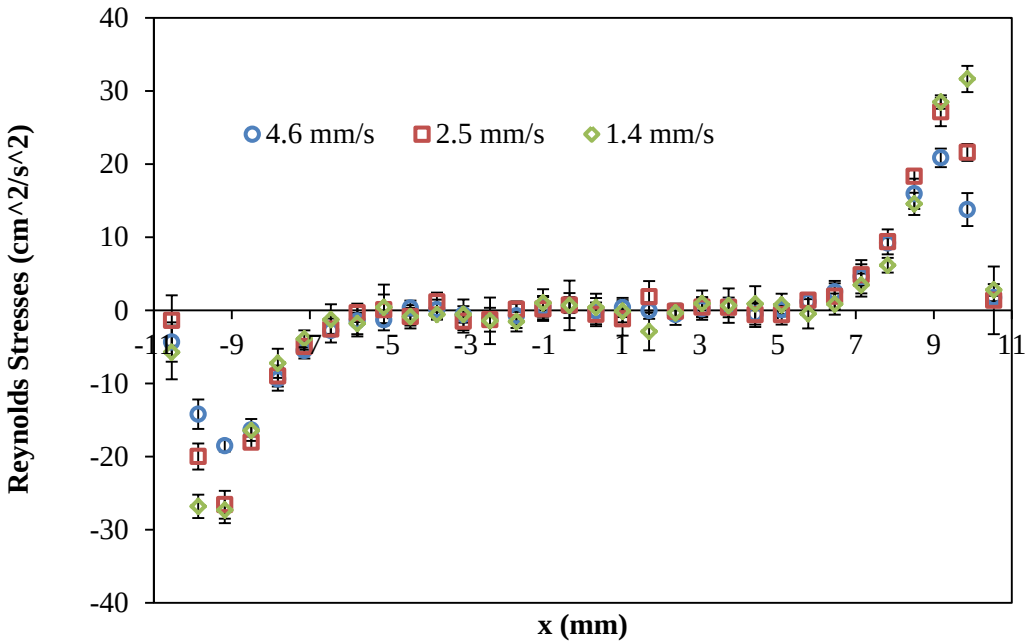

Fig. 15: Bubble Reynolds shear stresses obtained from Shadowgraphy.

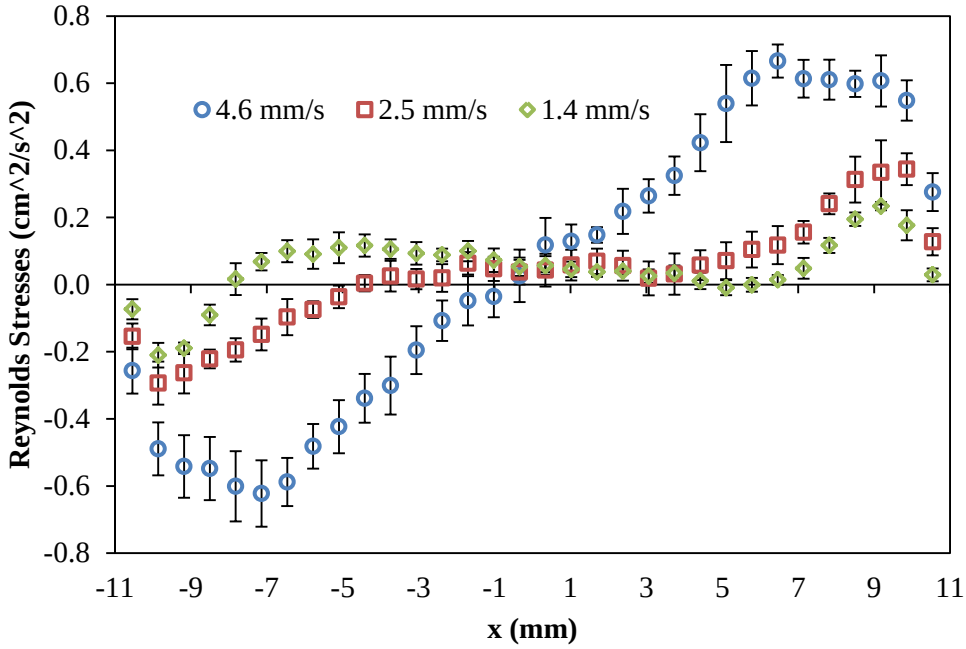

Fig. 16: Liquid Reynolds stresses obtained from PTV.

CONCLUSION

Three methods were successfully applied in this experiment to obtain two-phase flow parameters in a square channel. The study was performed in two regions far from the bubble injection location. The gas was inserted into the channel at three superficial gas velocities: 4.6 mm/s, 2.5 mm/s, and 1.4 mm/s. Using an in-house developed tracking algorithm, 2-D measurements were taken with PTV and shadowgraphy. PTV provided liquid parameters such as the velocity, RMS of the velocity, and Reynolds stresses. Shadowgraphy was able to provide gas parameters such as the centroid velocity, void fraction, size, RMS of the centroid velocity, and Reynolds stresses. Additionally, an optical probe was placed in the channel to measure the bubble interface velocity, void fraction, bubble frequency, time of flight, and Sauter mean diameter.

Most parameters were found to be in good agreement for both regions for all three methods. The only profiles from the optical probe results that displayed a difference between the two regions were the void fraction and interface velocity (resulting from the time of flight). In the shadowgraphy results the bubble centroid velocity for the second region was greater than for the first region. It is believed the bubbles were traveling faster in the second region as the low flow rate was not fully developed. The PTV results for the liquid phase showed changes between the two regions. The difference in the axial velocity profiles between the two regions was found to increase as the flow rate was reduced.

After concluding the experiment it was realized that the optical probe underestimates the gas phase parameters and shadowgraphy overestimates them, due to their measurement method. PTV was the most precise in its measurement method because only particles in the laser light

plane were tracked. It is believed the data obtained from this experiment will assist in improving and validating current simulations.